CAPITALIZING ON RELATIVE MOTION IN ELECTROSTATIC DETUMBLING OF AXI-SYMMETRIC GEO OBJECTS

Trevor Bennett and **Hanspeter Schaub**

6th International Conference on Astrodynamics Tools and Techniques (ICATT)

CAPITALIZING ON RELATIVE MOTION IN ELECTROSTATIC DETUMBLING OF AXI-SYMMETRIC GEO OBJECTS

T. Bennett, and H. Schaub[*]

University of Colorado Boulder
Aerospace Engineering Sciences
431 UCB, Colorado Center for Astrodynamics Research, Boulder, CO 80309-0431

ABSTRACT

Touchless methods of actuating and detumbling of large Earth-orbiting objects is of increasing importance for active debris mitigation strategies. Previously developed are electrostatic detumble dynamics and simulations for deep-space and lead-follower formations. This study investigates the influence of the instantaneous position and relative formation on electrostatic detumble performance. The mathematical sensitivities to relative position are developed to enable optimal relative guidance studies. The newly developed Linearized Relative Orbit Elements (LROE) formation flying controller is applied for formation maintenance. The benefits of formation flying in electrostatic detumble scenarios and the advantages of the LROE controller for electrostatic actuation applications are demonstrated through numerical simulations.

Index Terms— Electrostatic detumble, formation flying, relative motion control

1. INTRODUCTION

The Geostationary orbit (GEO) is one of the most valuable Earth orbiting regions requiring operators to maintain tight orbital slots and adhere to end-of-life practices to protect assets insured over 13 Billion US dollars.[1] The Geostationary belt is therefore a prime candidate for improved satellite servicing and removal strategies. Satellite servicing and debris removal are both challenging space mission concepts that require an active command vehicle to approach and mechanically interface with a defunct satellite or satellite component.[2-4] However, if the target object is tumbling at rates of up to 10's of degrees per second,[5] the process of docking onto the object exceeds current docking or grappling techniques and introduces additional collision risk. Advanced docking systems, such as those being developed by MacDonald Dettwiler and Associates (MDA), discuss a maximum tumble rate of 1 degree/second for autonomous docking.[6] If the target object tumble is lessened or removed, then existing grappling mechanisms could be utilized.

Electrostatic detumble addresses the present need of touchlessly detumbling target objects with additional applications in orbital servicing, fractionated satellite concepts, rendezvous and docking control, and many other proximity operations. Electrostatic actuation of spacecraft has been explored as early as the 1960s developing both the understanding of charging dynamics and electrostatic control for Earth-orbiting satellites.[7-13] In addition, electrostatic actuation with a passive object is being considered for both large GEO debris mitigation[14-17] as well as touchless asteroid spin control.[18,19] Specifically, Reference 20 shows that the Geosynchronous Orbit environment is a candidate region where space plasma conditions enable electrostatic interaction across 10's to 100's of meters requiring only Watt-levels of power. The electrostatic detumble mission concept, as shown in Figure 1, requires a servicing craft to modulate charge transfer via an electron or ion gun such that a differential electrostatic detumble torque is generated. Reference 21 first introduced how electrostatic charging can be controlled to apply torques on a spinning debris object without requiring physical contact as shown in Figure 1.
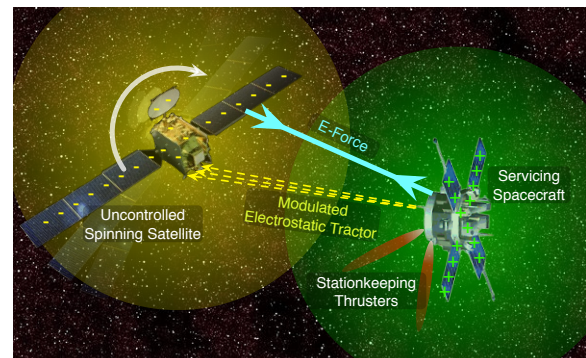

Fig. 1. Electrostatic actuation technology enabling diverse service mission profiles.

Electrostatic detumble control reduces the non-cooperative spacecraft rates prior to using other proximity or docking operations. Of particular interest to this study is a cylindrical target representative of booster upper stages, telescopes, and

---

[*]Alfred T. and Betty E. Look Professor of Engineering, Associate Chair of Graduate Affairs

dual-spin spacecraft. Reference 22 formulates the cylinder detumble control, the cylinder equations of motion, and shows the analytically predictable detumbled cylinder attitude and residual momentum given the initial momentum and a fixed servicer relative position. Further identified are specific attitudes where the servicer spacecraft has no electrostatic control authority on the cylinder tumble. To improve detumble performance, Reference 23 explores a lead-follower formation that removes additional angular momentum through systematic change in the relative position. It is shown that the lead-follower relative orbit completely detumbles the cylinder over the course of 11 days where the fixed servicer position is in general only capable of partial detumble. This concept is displayed in Figure 2 where the cylinder detumble is influenced by natural orbital motion. As Figure 2 illustrates,
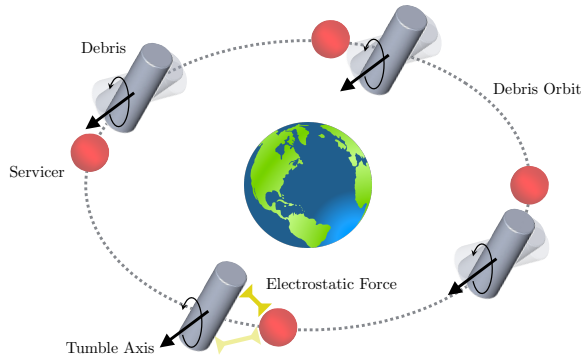

Fig. 2. Representative relative motion of servicer spacecraft around tumbling debris object.

the spherical servicer position relative to the angular momentum vector systematically changes throughout the orbit. The relative position shown at the bottom of Figure 2 highlights how differential torque is generated in an instantaneously favorable relative position. The time-varying inertial relative position change sweeps through alternate and favorable detumble configurations providing a more complete reduction in angular momentum.[23] While the lead-follower configuration is the most straight forward to implement, it may not be the most effective in terms of station keeping nor detumble time.

The current challenge is to distill the detumble-improving relative orbit from equations of motion that are a function of relative attitude and position. Earlier work explores charged formation flying with Coulomb debris tug trajectories[17,24] and use Coulomb and Lorentz forces.[25–27] However, this work maintains a prescribed relative orbit to address the advantages of formation flying on detumble performance. Utilized and developed in the following sections are the combination of the Linearized Relative Orbit Element (LROE) controller with previously developed cylindrical target charging models

to provide analytical relationships between relative orbit trajectories and detumble performance.

2. ELECTROSTATIC MODELING

The electrostatic interaction between two craft is accurately approximated for faster than real time control and simulation applications by the The Multi-Sphere Method (MSM). MSM represents the spacecraft electrostatic charging model as a collection of spherical conductors carefully dispersed through the body.[28] Consider a cylindrical target object representative of a spent upper-stage booster, a dual-spin spacecraft, or a variety of other spacecraft. The cylinder object is electrostatically manipulated by the collection of electrostatic forces induced by the presence of a charged spherical servicer spacecraft as shown in Figure 3. The presented 3-sphere MSM cylinder configuration is generated by matching the force, torque, and capacitance outputs of the commercial software package Maxwell for a variety of attitudes and ranges.[28] The
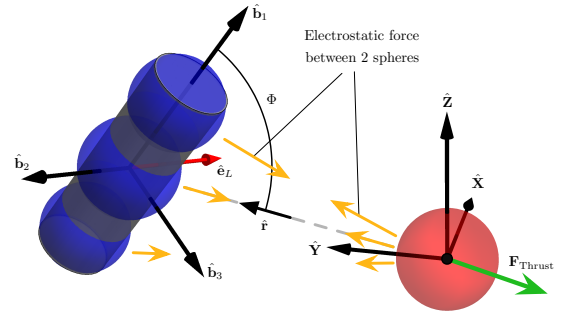

Fig. 3. 3 sphere MSM cylinder and spherical spacecraft configuration.

validated MSM model is used in faster-than-real-time simulations and control developments where the sphere-to-sphere electrostatic forces are determined by the charges residing on each sphere shown in Figure 3. The time-varying charges are computed from the prescribed electric potentials according to the self and mutual capacitance relationships in Eq. (1), where $k_c = 8.99 \times 10^9$ N·m^2/C^2 and q_i is the charge of each sphere.[29,30]

$$\phi_i = k_c \frac{q_i}{R_i} + \sum_{j=1, j \neq i}^{m} k_c \frac{q_j}{r_{i,j}} \qquad (1)$$

The term R_i denotes the radius of the ith conducting sphere and $r_{i,j}$ denotes the vector between the ith and j^{th} conducting spheres. These relations can be collected in matrix form

where a, b, c are the cylinder spheres' centers.

$$
\begin{bmatrix} \phi_1 \\ \phi_2 \\ \vdots \\ \phi_2 \end{bmatrix} = k_c \begin{bmatrix} 1/R_1 & 1/r_a & 1/r_b & 1/r_c \\ 1/r_a & 1/R_{2,a} & 1/l & 1/2l \\ 1/r_b & 1/l & 1/R_{2,b} & 1/l \\ 1/r_c & 1/2l & 1/l & 1/R_{2,c} \end{bmatrix} \begin{bmatrix} q_1 \\ q_a \\ q_b \\ q_c \end{bmatrix} \tag{2}
$$

Inverting the matrix multiplying the charge at a given instant in time produces the forces and torques on the cylinder given by the summations

$$
\boldsymbol{F}_2 = k_c q_1 \sum_{i=a}^{c} \frac{q_i}{r_i^3} \boldsymbol{r}_i \tag{3a}
$$

$$
\boldsymbol{L}_2 = k_c q_1 \sum_{i=a}^{c} \frac{q_i}{r_i^3} \boldsymbol{r}_{2,i} \times \boldsymbol{r}_i \tag{3b}
$$

Eq. (3b) provides the full MSM torque expression. However, the square matrix used to compute the charge has size equivalent to the number of MSM spheres and introduces a position-dependent coupling of the control potential ϕ to the sphere charges q_i. An analytic approximation of the MSM torque is utilized so that the control developments, the equilibrium states, and the stability of the system are more easily explored.[21,23]

2.1. The 3-Dimensional Detumble Coordinate Frame

The axi-symmetric cylinder and MSM sphere distribution shown in Figure 3 enable the control equations of motion to capture the charging behavior trends. Presented here are the equations of motion for the 3-dimensional detumble of an axi-symmetric MSM sphere distribution. In the MSM charging model case of a cylindrical target, no torque is generated on the roll rotation about the symmetric body axis $\hat{\boldsymbol{b}}_1$ due to the alignment of the spheres. Inspection of the torque produced by the MSM representation in Eq. (3b), the vector $\hat{\boldsymbol{r}}$ between the centers of mass of the two craft is always coplanar with the vectors from servicer sphere to all spheres of the cylinder. Torque is only produced about an axis perpendicular to the defined plane and thus the torque produced is always perpendicular to the vector $\hat{\boldsymbol{r}}$. It is therefore possible to define the torque axis $\hat{\boldsymbol{e}}_L$ and projection angle Φ about the torque axis

$$
\hat{\boldsymbol{e}}_L = \hat{\boldsymbol{b}}_1 \times (-\hat{\boldsymbol{r}}) \tag{4}
$$

$$
\Phi = \cos^{-1}\left(\hat{\boldsymbol{b}}_1 \cdot (-\hat{\boldsymbol{r}})\right) \tag{5}
$$

The vector $\hat{\boldsymbol{r}}$ is the unit separation vector from the servicing spacecraft mass center to the tumbling body mass center. The projection angle and torque axis are shown in Figure 3. A new coordinate frame $\mathcal{E} : \{\hat{\boldsymbol{b}}_1, \hat{\boldsymbol{e}}_L \times \hat{\boldsymbol{b}}_1, \hat{\boldsymbol{e}}_L\}$ is established with components shown in Figure 3.[22] The new coordinate frame isolates the torque influence such that the 3-dimensional torque vector is expressed as

$$
\boldsymbol{L} = L\hat{\boldsymbol{e}}_L \tag{6}
$$

For use in control developments, an analytical torque approximation that separates the potential and attitude information is first postulated in Reference 21 and is generalized to a 3-dimensional attitude projection Φ in Eq. (7).[31] This separation decouples the prescribed spacecraft potentials and the attitude information enabling control developments to focus on relative attitude.

$$
L = \gamma f(\phi) g(\Phi) \tag{7}
$$

with $g(\Phi)$ assuming the following form for an axi-symmetric cylinder

$$
g(\Phi) = \sin(2\Phi) \tag{8}
$$

The proposed detumble controller assumes the projection angle Φ and rate $\dot{\Phi}$ are measured and the servicer spacecraft potential ϕ_1 is the control variable.[22] The prescribed potential control $f(\phi_1)$

$$
f(\phi_1) = -\text{sgn}\left(g(\Phi)\right) f(\phi_{\max}) \frac{\arctan(\alpha\dot{\Phi})}{\pi/2} \tag{9}
$$

where $\alpha > 0$ is a constant feedback gain and $\phi_{\max}$ has values in the 20-30 kV range. Eq. (8) reveals that there are some attitudes for the 3-sphere cylinder that are zero-torque cases as well as attitudes that maximize the torque. The prospect of utilizing relative motion to maximize favorable detumble attitudes is what motivates this formation flying electrostatic detumble study.

2.2. Electrostatic Detumble Equations of Motion

While the controller could extract the projection angle at every time step, it is more convenient to rewrite the equations of motion in terms of the projection angle and relative position. The $\mathcal{E}$-frame, with components shown in Figure 3, provides a convenient frame in which to express the rotational equations of motion.[22] Note that the moment of inertia about the torque axis $\hat{\boldsymbol{e}}_L$ is always perpendicular to $\hat{\boldsymbol{b}}_1$.

$$
I_a \dot{\omega}_1 = 0 \tag{10a}
$$

$$
I_t \dot{\eta} - I_a \omega_1 \dot{\Phi} \sin\Phi = 0 \tag{10b}
$$

$$
I_t \left(\ddot{\Phi} \sin\Phi - \eta^2 \frac{\cos\Phi}{\sin^2\Phi} \right) + I_a \omega_1 \eta = L \tag{10c}
$$

Representing the equations of motion in the projection angle coordinate system $\mathcal{E}$ shows that the control only influences torques around the cylinder's transverse $\hat{\boldsymbol{e}}_L$ axis. Consistent with the assumption of an axi-symmetric geometry, there exists no control authority in the $\hat{\boldsymbol{b}}_1$ axis scalar equation and no cross coupling is present. Thus, ω_1 is constant for all time. In Eq. (10), the angular velocity measures η and $\dot{\Phi}$, as well as the electrostatic control torque $\boldsymbol{L}$, are defined by

$$
\eta \equiv -\omega_2(\hat{\boldsymbol{r}} \cdot \hat{\boldsymbol{b}}_2) - \omega_3(\hat{\boldsymbol{r}} \cdot \hat{\boldsymbol{b}}_3) \tag{11a}
$$

$$
\dot{\Phi} \sin\Phi = -\omega_2(\hat{\boldsymbol{r}} \cdot \hat{\boldsymbol{b}}_3) + \omega_3(\hat{\boldsymbol{r}} \cdot \hat{\boldsymbol{b}}_2) \tag{11b}
$$

$$
\boldsymbol{L} = -L\hat{\boldsymbol{e}}_L = -\gamma f(\phi) g(\Phi) \hat{\boldsymbol{e}}_L \tag{11c}
$$

The equations of motion shown in Eq. (10) provide significant insight into the detumble steady-state behavior and introduce the opportunity for detumble optimization.

2.3. Considerations for Dynamics as Seen by the Hill Frame

The equations of motion in Eq. (10) are derived assuming that the relative position of the spacecraft is fixed in the inertial frame, thus allowing the more simplified form.[22] Desired is a study of various relative orbit geometries that improve the detumble performance while on orbit motivated by the thought experiment in Figure 2. As discussed in Reference 23, the tumbling dynamics of the target cylinder are much faster than the change in relative position while in GEO orbit. Therefore, the presented equations of motion are valid while the tumble rate is much larger than the relative position rate. This assumption is further discussed in the results of the numerical simulations.

The angular momentum as seen by the Hill frame must also be considered for relative orbit optimization. In the absence of perturbations, the inertially-fixed angular momentum vector $\boldsymbol{H}$ appears to cone in the rotating Hill frame in accordance with $H^{\mathcal{H}} = [HN]H^{\mathcal{N}}$. This is exemplified in Figure 4 where the target cylinder is the center of the Hill frame and the servicer position is controlled.
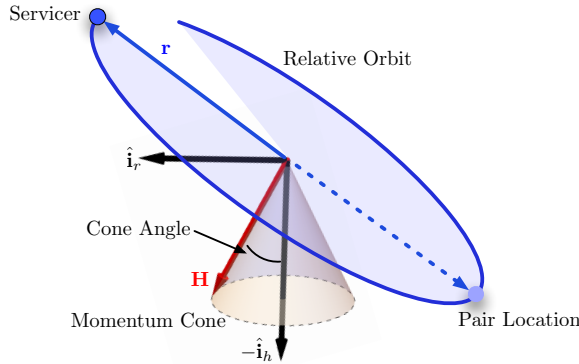

Fig. 4. Representation of the angular momentum coning present in the Hill frame.

The relative orbit as seen in the Hill frame $\mathcal{H} = [\hat{\boldsymbol{i}}_r, \hat{\boldsymbol{i}}_\theta, \hat{\boldsymbol{i}}_h]$ is shown in Figure 4 as the blue swept relative ellipse. The inertially fixed angular momentum vector $\boldsymbol{H}$ precesses through a cone centered on the Hill frame orbit normal. The precession of this vector is leveraged to inform a relative orbit that enhances the detumble performance. This study provides the development for a relative motion optimization approach that delivers the servicer relative motion to achieve the desired performance increase. The optimizer also provides a

pair location that will be discussed in greater detail in following sections.

The coning motion is critical to determining more time optimal detumble solutions. Consider the fundamental form of Euler's equations where $\dot{\boldsymbol{H}} = \boldsymbol{L}$. As described by the previous section, the electrostatic torque is only generated perpendicular to the servicer relative position. It is advantageous to determine a relative orbit that drives the servicer relative position to be perpendicular to the Hill frame angular momentum. Therefore, the presented study generalizes the angular momentum as seen by the Hill frame to a combination of a cone angle and phase angle. The relative orbit optimization insight gained through optimization is generally applicable to all orbit inclinations. The following section introduces the relative orbit coordinates used followed by a section that develops the optimization approach.

3. GUIDANCE AND CONTROL USING LINEARIZED RELATIVE ORBIT ELEMENTS

Motivated are relative orbits that capitalize on the natural relative motion of orbiting formations to improve the detumble performance. Considered by this study are detumble targets in the Geostationary (GEO) orbit regime which is a prime candidate for applying the Clohessy-Wiltshire (CW) relative orbit equations.[32] While the CW equations provide a suitable relative position description, the newly developed guidance and control methodology using the CW integration constants is utilized.[33] A slight modification to the CW equations removes the α and β ambiguity through trigonometric expansion and largely preserves the inherent insight. The modified non-singular CW equations are

$$x(t) = A_1 \cos(nt) - A_2 \sin(nt) + x_{\text{off}} \tag{12a}$$

$$y(t) = -2A_1 \sin(nt) - 2A_2 \cos(nt) - \frac{3}{2}nt x_{\text{off}} + y_{\text{off}} \tag{12b}$$

$$z(t) = B_1 \cos(nt) - B_2 \sin(nt) \tag{12c}$$

The state vector for Linearized Relative Orbit Element (LROE) guidance is the collection of the CW equations' integration constants not the Cartesian state. The LROE form provides the relative motion geometry in the absence of perturbations where these parameters remain constant. The nominally invariant nonsingular LROE state vector $\boldsymbol{X}_{\text{NS}}$, defined as

$$\boldsymbol{X} = [A_1, A_2, x_{\text{off}}, y_{\text{off}}, B_1, B_2] \tag{13}$$

First derived in Reference 33, the dynamics of the LROE state in the presence of perturbations can be obtained by applying Lagrange Brackets to the non-singular LROE equations. This approach is analogous to Lagrange's planetary equations in that the LROE set becomes osculating to match the perturbed relative orbit. The nonsingular state vector in Eq. (13) evolves

according to Eq. (14) where $\boldsymbol{a}_d$ is the disturbance acceleration in the Hill frame.[33]

$$\dot{\boldsymbol{X}} = \frac{1}{n} \underbrace{\begin{bmatrix} -\sin(nt) & -2\cos(nt) & 0 \\ -\cos(nt) & 2\sin(nt) & 0 \\ 0 & 2 & 0 \\ -2 & 3nt & 0 \\ 0 & 0 & -\sin(nt) \\ 0 & 0 & -\cos(nt) \end{bmatrix}}_{B(\boldsymbol{X},t)} \begin{bmatrix} a_x \\ a_y \\ a_z \end{bmatrix} \quad (14)$$

Given that the LROE state evolves from perturbation accelerations, a Psuedo-Inverse relative motion controller is applied to achieve the desired relative orbit by injecting a control acceleration into Eq. (14). The LROE state error can be defined as

$$\Delta\boldsymbol{æ} = \boldsymbol{X} - \boldsymbol{X}_r \quad (15a)$$

$$\Delta\dot{\boldsymbol{æ}} = \dot{\boldsymbol{X}} - \dot{\boldsymbol{X}}_r = [B](\boldsymbol{u} - \boldsymbol{u}_r) \quad (15b)$$

where the $()_r$ denotes the reference trajectory. The time rate of the LROE error measure also allows the reference trajectory to be defined by a LROE rate. Shown in Reference 33, the Lyapunov asymptotically-stable feedback control law is

$$\boldsymbol{u} = -([B]^T[B])^{-1}[B]^T[K]\Delta\boldsymbol{æ} \quad (16)$$

The simple feedback form allows the implemented control to apply a corrective acceleration to maintain the desired relative orbit in the presence of perturbations. Consider the effect of the electrostatic force during proximity electrostatic interaction between the servicer as the deputy object with the target cylinder at the origin of the Hill coordinate frame. The attractive and repulsive forces on the servicer will perturb the relative orbit of the servicer about the target object. The current study utilizes the control form in Eq. (16) to maintain the desired relative orbit in the presence of electrostatic forces. In addition, the guidance control enables feed-forward of perturbation accelerations.

The gain developed for the LROE controller in previous studies is set to

$$[K] = (n \cdot 10^4) \times \text{diag}([1, \ 1, \ 30, \ 1, \ 1, \ 1]) \quad (17)$$

The gain matrix utilized may not be optimal, however sufficient performance is obtained. Future studies will address the gain matrix and seek dynamical system leverage in scaling the gain values.

4. LROE RELATIVE ORBIT OPTIMIZATION FOR DETUMBLE PERFORMANCE

Desired is a relative orbit that provides enhanced detumble performance over the lead-follower or other relative orbit types. The following approach weights the separation distance and the instantaneous servicer positions to optimize a single relative orbit for the duration of the detumble period. As shown in Eq. (3b), the available electrostatic torque is inversely proportional to the squared separation distance. Therefore, minimizing the separation distance with an operationally acceptable lower bound ensures the greatest opportunity for maximizing detumble torque. Second, the most effective reduction in angular momentum exists when the torque is anti-parallel to the angular momentum vector. As shown in previous sections, the electrostatic torque is perpendicular to the servicer relative position suggesting that the relative position should reside as close to perpendicular to the angular momentum vector as possible. A cost function to capture these considerations is considered here. The objective is to minimize the time to detumble not necessarily the station-keeping fuel cost. However, the resulting station-keeping cost is explored through numerical simulations.

The proposed optimization approach leverages MATLAB's *fmincon* optimizer. While many optimization toolboxes exist, *fmincon* provides the state bounds, simplicity of implementation, and wealth of documentation to provide a sufficient first analysis of the desired approach. The following optimization approach requires a robustness addition because MATLAB's *fmincon* optimizer does not guarantee a global minimum.

4.1. Relative Orbit Cost Function and State Bounds

Proposed is an optimization cost function that minimizes both the separation distance and minimizes the off-perpendicular alignment of the relative position and momentum vector. First considered is a cost function that utilizes just the torque obtained for the particular relative position and attitudes about the angular momentum vector. However, this approach introduces local minima because the cost function relies on a sweep of attitudes and additional discretization assumptions. Therefore, a more general cost function that does not require instantaneous attitude information is explored to help reduce the number of local minima.

$$J = \sum_{i=0}^{N} \left(-1000 \ln[|\boldsymbol{r}_i| - r^* + 1] - 10 \ln\left[\left|\frac{\boldsymbol{r}_i \cdot \boldsymbol{H}_i}{\|\boldsymbol{r}_i\|\|\boldsymbol{H}_i\|}\right| + 1\right] \right) \quad (18)$$

The cost in EQ. (18) is accumulated over a single discretized relative orbit with N time segments. This study utilizes 50 uniform time segments. The relative position and angular momentum are expressed in the Hill frame where $\boldsymbol{r}_i = \boldsymbol{r}(t_i)$ and $\boldsymbol{H}_i = \boldsymbol{H}(t_i)$ at time t_i. The minimum separation distance is prescribed by r^*. The relative weights are selected to achieve the same order of magnitude contribution for both separation distance and angle error. Both values are increased by an order of magnitude to help the convergence characteristics of the *fmincon* optimizer.

Only positive values of the LROE state are considered. This limits the relative orbit space to only the positive combinations, however it captures the full space in the cost function.

The cosine cost, from the dot product, is symmetric about $\pi/2$ radians. Recall that the angular momentum traces a cone as viewed in the Hill frame over a single orbit. The cost function seeks a relative position vector that is perpendicular to the angular momentum vector. This is achieved by the absolute value of the dot product approaching zero. Consider a relative orbit plane with a normal parallel to the centerline of the angular momentum cone as shown in Figure 4. Should the servicer reside in either point separated by a relative orbit phase angle of π, then both points will have equivalent cost because both points provide equivalent cosine angle magnitudes relative to the instantaneous angular momentum vector. This allows the LROE state search to be reduced to a subset of all available LROE combinations where the symmetry can be later invoked to create pairs of optimized relative orbits.

In addition, the relative orbit should remain bounded for the duration of the detumble mission segment. The radial offset x_{off} is set to zero for all time to retain the bounded relative orbit. The desired minimum separation distance is at least four times the target craft radii. The cylinder considered by this study has 3 meters as the largest dimension setting the minimum separation distance to $r^* = 12.5$ meters. The remaining LROE states are initialized at 15 meters with an arbitrarily large upper bound of 40 meters and lower bound of 0 meters to keep all values positive.

4.2. Proposed Relative Orbit Schema

The optimization space is first explored using a sweep of the available relative orbit configurations for the possible angular momentum configurations. Referring to Figure 4, the angular momentum is parameterized by a cone angle that is measured from the orbit normal and a phase angle that is measured from the positive $\hat{x}$ axis in the Hill frame. Sweeping through the unique momentum vectors that reside in a cone angle in [0,90] and a phase angle in [0,360), the resulting cost of Eq. (18) drives the LROE state to the values in Figure 5. The optimized
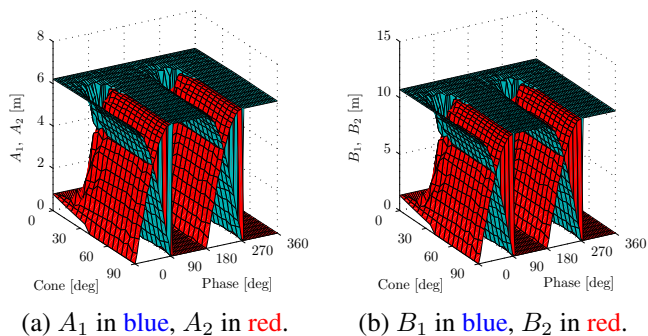

(a) A_1 in blue, A_2 in red.   (b) B_1 in blue, B_2 in red.

Fig. 5. Optimization output demonstrating clear LROE optimums.

LROE values for the planar A_i terms and the out-of-plane B_i

terms is shown in Figures 4.2 and 4.2 respectively with the first term in blue. Initial observation reveals that the resulting terms have similar structure in the phase angle which is to be expected. Further, considering that the inclined orbit plane represented in Figure 4 provides better torque geometry for larger cone angles is consistent with the strong trends above a cone angle of 40 degrees in Figure 5. Also interesting is the results for values of a cone angle less than 30 degrees. The optimizer did not produce globally optimal results where the term y_{off} was not well captured by the cost function due to local minima. However, the the geometrical insight from Figure 4 suggests that a lead-follower may be most optimal in this region. Given the insight by Figure 5, robustness is added by comparing the lead-follower cost for any formation that has an angular momentum cone angle less than about 30-40 degrees.

The restriction to only positive LROE state values enables the clear character visible in Figure 5. As seen in Figure 4, there is a pair LROE location that resides on the opposite side, a phasing difference of π, of the relative orbit that provides the same relative separation and geometry. Using the symmetry of phasing, the results in Figure 5 provide both the primary and pair relative orbit solutions.

The optimized values for the relative orbit were achieved by constraining the minimum separation distance to 12.5 meters. However, the results shown in Figure 5 are applicable to any minimum separation distance. The LROE set are constants and scale to any relative orbit size. Therefore the relative proportions are the key insight achieved by the optimization results.

5. DETUMBLE PERFORMANCE FOR SELECT CONE ANGLES

Two numerical simulations are performed to validate the GEO orbit detumble performance achieved using optimized relative orbit trajectories. The simulation initializes the servicer spacecraft 12.5 meters away from a generally tumbling cylinder using the optimized output state. The numerical simulation includes the 6-DOF motion of the debris and 3-DOF translational motion of the servicer sphere. The closed-loop feedback control in Eq. (16) is used to maintain a fixed relative position between servicer and debris. A 4th order Runge-Kutta integration is employed with a time step of 0.01 seconds for 14 days. The servicer vehicle potential is controlled via Eq. (9) and the charging model in Reference 34, while the electrostatic force is evaluated using the full MSM model in Eqs. (2)–(3b). Additional simulation values are included in Table 1.

Considered are two cone angles of the angular momentum as seen by the Hill frame. The rotating Hill frame and the inertial reference frame are coincident during initialization. The first case is initialized with a cone angle of $79°$ from an angular momentum of $\boldsymbol{H} = [-26.7,\ 1.091,\ -7.16]$ [N-m-s]. This

Table 1. Simulation parameters for cylinder detumble system.

Parameter	Value	Units	Description
R_1	2	m	Servicer radius
m_1	500	kg	Servicer mass
m_2	1000	kg	Cylinder mass
I_a	125.0	kg·m^2	Axial inertia
I_t	812.5	kg·m^2	Transverse inertia
ω_0	2	deg/sec	Cylinder tumble
α	5×10^4	-	Control Gain
ϕ_{max}	20	kV	Max voltage

represents a large cone angle and the optimized LROE state is expected to exceed the performance of the lead-follower state. The second case is initialized with a cone angle of $22.5°$ from an angular momentum of $\boldsymbol{H} = [-7.656, -4.0769, -26.27]$ [N-m-s]. This represents a smaller cone angle where the lead-follower is expected to exceed the out-of-plane optimizer output state. The cases are examined in greater detail below.

5.1. Large Cone Angle - Optimized LROE Proposed

The first case considers a large cone angle of $79°$ to illustrate the advantage of implementing an LROE optimized state over a simple lead-follower. Using the *fmincon* optimization approach, the LROE state and lead-follower state are set to

$$\boldsymbol{X} = [A_1, A_2, x_{\text{off}}, y_{\text{off}}, B_1, B_2] \text{ [m]}$$
$$\boldsymbol{X}_0^{\text{opt}} = [0, 6.25, 0, 0, 0, 10.83] \text{ [m]}$$
$$\boldsymbol{X}_0^{\text{lf}} = [0, 0, 0, 12.5, 0, 0] \text{ [m]}$$

Utilizing the LROE control scheme over the 14 day simulation period, the optimized LROE orbit and the lead-follower orbit follow the paths shown in Figure 6. The LROE controller keeps the relative orbit close to the desired state through feedback control. Implementation of a more aggressive control would reduce the state error further if desired.

Of interest is the detumble performance for the respective LROE states. The electrostatic detumble reduction in the angular momentum is shown in Figure 7 where both the lead-follower and optimized state histories are shown.

Initial inspection of the angular momentum reduction in Figure 7 reveals that the optimized state completes the primary detumble in close to 180 hours where the lead-follower requires closer to 220 hours. Following the primary detumble phase, both relative orbits experience fluctuations while further reducing the angular momentum. Recall that the projection angle detumble equations assume that the relative position is not changing or changes much slower than the tumble rate. This assumption is valid during the primary detumble phase exemplified by clear and monotonic decrease in angular momentum magnitude. However, as the tumble slows to a
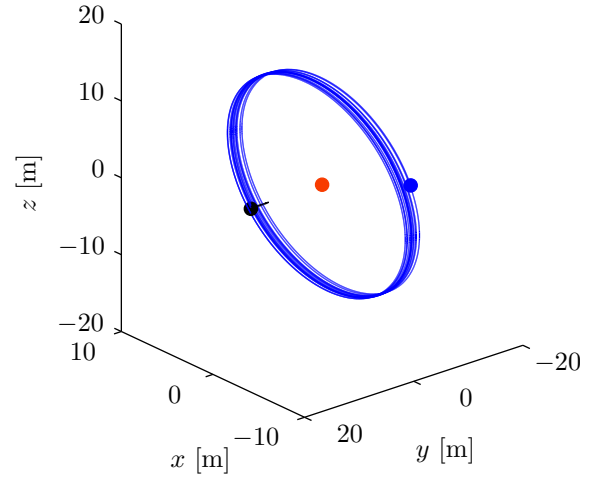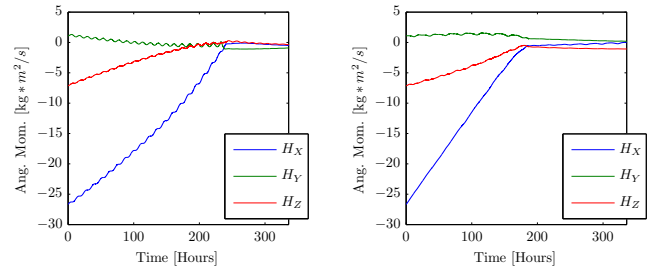

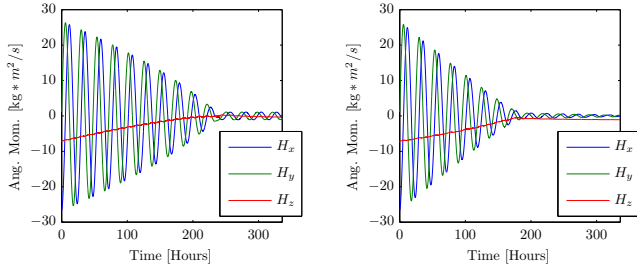**Fig. 6**. The optimized state in blue and the lead-follower in black.

(a) Lead-follower configuration.   (b) Optimized LROE orbit.

Fig. 7. Comparison in the detumble performance for a large cone angle.

rate that is more on the order of magnitude as the change in relative position, the projection angle change is no longer primarily a function of cylinder body attitude rates. Inspection of the final detumble phase demonstrates the deterioration of the global stability arguments provided during the primary detumble phase.

Also of interest is the reduction in angular momentum as seen by the Hill frame. Recall that the optimization approach leverages the revolution of the angular momentum in the Hill frame to design a relative trajectory. The electrostatic detumble angular momentum reduction as seen by the Hill frame is shown in Figure 8. Inspection of Figure 8 reveals that the optimized ellipse delivers a more complete detumble in the radial and transverse directions where the lead-follower provides more complete reduction of the orbit-normal angular momentum. This is consistent with the relative position advantages where the lead-follower is most often perpendicular

(a) Lead-follower configuration. (b) Optimized LROE orbit.

Fig. 8. Hill frame detumble performance for a large cone angle.

to the orbit normal where the optimized state provides a relative position that is more perpendicular to the orbit radial and along-track directions. This alignment is further seen in Figure 5.1 where the cross product between the relative position and angular momentum vector is shown. Note that best detumble alignment occurs when the relative position vector is perpendicular to the angular momentum vector: a cross product of unity. The cyclic nature of the relative orbit emerges in the cyclic drops in alignment benefit. Further inspection of Figure 5.1 demonstrates that the cross product becomes wildly variable for the optimized state following the transition from primary to secondary detumble phases. This transition suggests that the optimization approach could be re-applied to obtain a new optimized LROE state and that the LROE controller could be used to transition to the new state. The station-
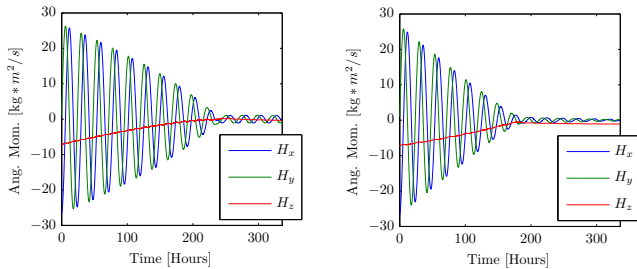
(a) Lead-follower and Optimized. (b) Orbit maintenance total.

Fig. 9. Detumble geometry and orbit maintenance for a large cone angle.

keeping acceleration for both the lead-follower and the optimized state is shown in Figure 9. The transition from primary to secondary detumble phases is clearly jointed for both LROE states. The total acceleration is comparable between the two relative orbits. However, the variation in the relative orbit seen in Figure 6 suggests that the control gain should be more aggressive to reduce the variation in the state due to the electrostatic perturbations. A more aggressive controller may exaggerate the acceleration requirement differences between

the two states. In addition, the control implemented is only a feedback control where the provided LROE form enables feed-forward capability.

Exhibited by the large cone angle angular momentum reduction in Figure 7 is the detumble time benefit of using an optimized relative orbit. Further demonstrated by Figure 5.1 is that the optimization approach is consistent with the performance output. Further demonstrated is the use of the LROE state for both guidance and control for electrostatic detumble applications. The second case provides an additional example the further capitalizes on the insight inherent in using an LROE state.

5.2. Small Cone Angle - Lead Follower Proposed

The second case considers a small angular momentum cone as seen in the Hill frame. The resulting optimized state is achieved using the optimization approach. The small cone angle relative orbit as seen in the Hill frame is so similar to Figure 6 that it is not shown here.

$$\boldsymbol{X} = [A_1, A_2, x_{\text{off}}, y_{\text{off}}, B_1, B_2] \text{ [m]}$$
$$\boldsymbol{X}_0^{\text{opt}} = [0.95, \ 6.2, \ 0, \ 0, \ 1.64, \ 10.7] \text{ [m]}$$
$$\boldsymbol{X}_0^{\text{lf}} = [0, \ 0, \ 0, \ 12.5, \ 0, \ 0] \text{ [m]}$$

The small angular momentum cone introduces local minima into the cost function. Therefore, the optimized relative orbit state for the small cone angle is similar to that of the large cone angle. Intuition suggests that with a smaller cone angle, the relative orbit should approach a lead-follower noting that the lead-follower is best for a cone angle of zero. The relative orbit cost minima are a result of the orbital dynamics captured in the CW equations. The planar relative orbits assume 2-1 ellipses as seen by the coefficients in Eq. (12). The detumble performance is maximized first by minimizing the separation distance between the two craft. Allowing the optimizer to consider out-of-plane motion provides a local minima where the separation distance is constant at the minimum possible, however the alignment between the relative position vector and angular momentum vector is sub-optimal. All relative orbits around the optimizer local minimum introduces greater separation distances keeping the optimized state at the local minima. Returning to Figure 5 shows the transition between the optimization output and the probable lead-follower global minima between the 30-40 degree cone angle range. This interpretation of the optimizer output is explored using a smaller cone angle.

The detumble performance when a smaller angular momentum cone angle exists is shown in Figure 10. The lead-follower provides a time reduction of nearly 100 operational hours to complete the primary detumble phase. This is further demonstrated in Figure 11 by observing the angular momentum as seen by the Hill frame.
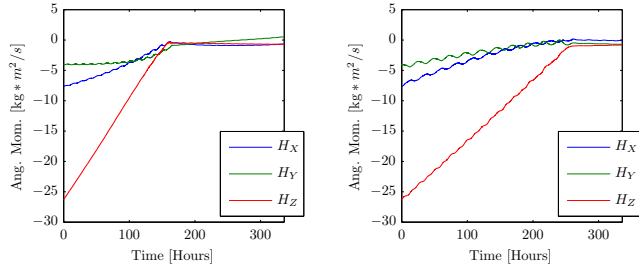
(a) Lead-follower configuration.   (b) Optimized LROE orbit.

Fig. 10. Comparison in the detumble performance for a large cone angle.
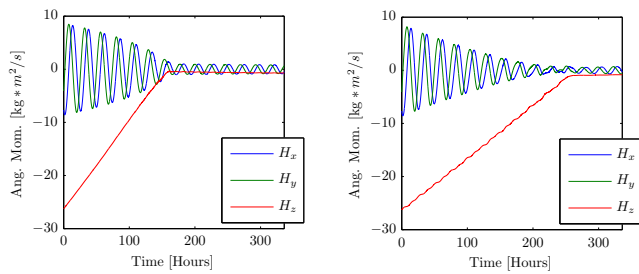
(a) Lead-follower and Optimized.   (b) Orbit maintenance total.

Fig. 11. Detumble geometry and orbit maintenance for a small cone angle.

Exhibited by a smaller angular momentum cone angle is the advantage of using a lead-follower over a relative orbit that includes out-of-plane motion. However, a properly phased out-of-plane relative orbit may introduce additional operational safety by providing a safety ellipse in the case of discontinued control. The control acceleration is also of the same magnitude for both relative orbit types given that that total angular momentum removed is almost identical. Achieved through comparing two angular momentum cone angles is the advantage of using different relative orbits for different angular momentum configurations.

6. CONCLUSIONS

Electrostatic detumble is significantly influenced by the relative position of the servicer craft. Initial investigation demonstrates there are performance gains and losses due to the initial phasing and relative orbit type. This study further investigates the axi-symmetric cylinder electrostatic detumble performance with a time-varying relative position controlled by the recently developed Linearized Relative Orbit Elements (LROEs) formulation. Given the optimization sweep over the angular momentum cone space, the lead-follower is used for any formation that has an angular momentum cone angle less

than about 30-40 degrees where the optimized LROE state is used otherwise. As shown by the numerical simulations, the use of relative motion enables near-complete detumble of 2°/sec rocket body tumble in as little as 7 operation days. The lead-follower relative orbit provides sufficient detumble performance for limited relative orbit complexity. However, the optimized relative orbit may provide a reduction of days in detumble operation time. In addition, the ease of transitioning between relative orbit types with the LROE control provides an opportunity to utilize several relative orbits during a single detumble period.

7. ACKNOWLEDGEMENTS

8. REFERENCES

[1] Philip Chrystal, Darren McKnight, Pamela L. Meredith, Jan Schmidt, Marcel Fok, and Charles Wetton, "Space debris: On collision course for insurers?," Tech. Rep., Swiss Reinsurance Company Ltd, Zürich, Switzerland, March 2011.

[2] Patrice Couzin, Frank Teti, and R. Rembala, "Active removal of large debris: System approach of de-orbiting concepts and technological issues," in *6th European Conference on Space Debris*, Darmstadt, Germany, April 22–25 2013, Paper No. 6a.P-17.

[3] Andrew Ogilvie, Justin Allport, Michael Hannah, and John Lymer, "Autonomous satellite servicing using the orbital express demonstration manipulator system," in *Proc. of the 9th International Symposium on Artificial Intelligence, Robotics and Automation in Space (i-SAIRAS'08)*, 2008, pp. 25–29.

[4] Wenfu Xu, Bin Liang, Bing Li, and Yangsheng Xu, "A universal on-orbit servicing system used in the geostationary orbit," *Advances in Space Research*, vol. 48, no. 1, pp. 95–119, 2011.

[5] Yu S. Karavaev, R. M Kopyatkevich, M. N. Mishina, G. S. Mishin, P. G. Papushev, and P. N. Shaburov, "The dynamic properties of rotation and optical characteristics of space debris at geostationary orbit," in *Advances in the Astronautical Sciences*, 2004, vol. 119, pp. 1457–1466, Paper No. AAS-04-192.

[6] Patrice Couzin, Frank Teti, and Richard Rembala, "Active removal of large debris : Rendez-vous and robotic capture issues," in *2nd European Workshop on Active Debris Removal*, Paris, France, 2012, Paper #7.5.

[7] Lyon B. King, Gordon G. Parker, Satwik Deshmukh, and Jer-Hong Chong, "Spacecraft formation-flying using inter-vehicle coulomb forces," Tech. Rep., NASA/NIAC, January 2002, http://www.niac.usra.edu.

[8] John Berryman and Hanspeter Schaub, "Analytical charge analysis for 2- and 3-craft coulomb formations," *AIAA Journal of Guidance, Control, and Dynamics*, vol. 30, no. 6, pp. 1701–1710, Nov.–Dec. 2007.

[9] Carl R. Seubert, Stephan Panosian, and Hanspeter Schaub, "Analysis of a tethered coulomb structure applied to close proximity situational awareness," *AIAA Journal of Spacecraft and Rockets*, vol. 49, no. 6, pp. 1183–1193, Nov. – Dec. 2012.

[10] Laura A. Stiles, Hanspeter Schaub, Kurt K. Maute, and Daniel F. Moorer, "Electrostatically inflated gossamer space structure voltage requirements due to orbital perturbations," *Acta Astronautica*, vol. 84, pp. 109–121, Mar.–Apr. 2013.

[11] Shuquan Wang and Hanspeter Schaub, "Nonlinear charge control for a collinear fixed shape three-craft equilibrium," *AIAA Journal of Guidance, Control, and Dynamics*, vol. 34, no. 2, pp. 359–366, Mar.–Apr. 2011.

[12] Mason A. Peck, "Prospects and challenges for lorentz-augmented orbits," in *AIAA Guidance, Navigation and Control Conference*, San Francisco, CA, August 15–18 2005, Paper No. AIAA 2005-5995.

[13] Brett Streetman and Mason A. Peck, "New synchronous orbits using the geomagentic lorentz force," *AIAA Journal of Guidance, Control, and Dynamics*, vol. 30, no. 6, pp. 1677–1690, Nov.–Dec. 2007.

[14] Hanspeter Schaub and Daniel F. Moorer, "Geosynchronous large debris reorbiter: Challenges and prospects," in *AAS Kyle T. Alfriend Astrodynamics Symposium*, Monterey, CA, May 17–19 2010, Paper No. AAS 10-311.

[15] Daniel F. Moorer and Hanspeter Schaub, "Hybrid electrostatic space tug," US Patent 0036951-A1, Feb. 17 2011.

[16] Daniel F. Moorer and Hanspeter Schaub, "Electrostatic spacecraft reorbiter," US Patent 8,205,838 B2, Feb. 17 2011.

[17] Erik Hogan and Hanspeter Schaub, "Space debris reorbiting using electrostatic actuation," in *AAS Guidance and Control Conference*, Breckenridge, CO, Feb. 3–8 2012, Paper AAS 12–016.

[18] Naomi Murdoch, Dario Izzo, Claudio Bombardelli, Ian Carnelli, Alain Hilgers, and David Rodgers, "Electrostatic tractor for near earth object deflection," in *59th International Astronautical Congress*, Glasgow Scotland, 2008, Paper IAC-08-A3.I.5.

[19] Naomi Murdoch, Dario Izzo, Claudio Bombardelli, Ian Carnelli, Alain Hilgers, and David Rodgers, "The electrostatic tractor for asteroid deflection," in *58th International Astronautical Congress*, 2008, Paper IAC-08-A3.I.5.

[20] John H. Cover, Wolfgang Knauer, and Hans A. Maurer, "Lightweight reflecting structures utilizing electrostatic inflation," US Patent 3,546,706, October 1966.

[21] Hanspeter Schaub and Daan Stevenson, "Prospects of relative attitude control using coulomb actuation," in *Jer-Nan Juang Astrodynamics Symposium*, College Station, TX, June 25–26 2012, Paper AAS 12–607.

[22] Trevor Bennett and Hanspeter Schaub, "Touchless electrostatic three-dimensional detumbling of large axi-symmetric debris," *Journal of Astronautical Sciences*.

[23] Trevor Bennett and Hanspeter Schaub, "Touchless electrostatic detumbling while tugging large axi-symmetric geo debris," in *25th AAS/AIAA Spaceflight Mechanics Meeting*, Williamsburg, Virginia, Jan. 11–15 2015, Paper AAS 15-383.

[24] Erik Hogan and Hanspeter Schaub, "Relative motion control for two-spacecraft electrostatic orbit corrections," *AIAA Journal of Guidance, Control, and Dynamics*, vol. 36, no. 1, pp. 240–249, Jan. – Feb. 2013.

[25] Utako Yamamoto and Hiroshi Yamakawa, "Two-craft coulomb-force formation dynamics and stability analysis with debye length characteristics," in *AIAA/AAS Astrodynamics Specialist Conference and Exhibit*, Honolulu, Hawaii, Aug. 18–21 2008, Paper No. AIAA 2008-7361.

[26] M. A. Peck, B. Streetman, C. M. Saaj, and V. Lappas, "Spacecraft formation flying using lorentz forces," *Journal of British Interplanetary Society*, vol. 60, pp. 263–267, July 2007.

[27] Hiroshi Yamakawa, Mai Bando, Katsuyuki Yano, and Shu Tsujii, "Spacecraft relative dynamics under the influence of geomagnetic lorentz force," in *AIAA Guidance, Navigation and Control Conference*, Toronto, Canada, Aug. 2–5 2010, Paper No. AIAA 2010-8128.

[28] Daan Stevenson and Hanspeter Schaub, "Multi-sphere method for modeling electrostatic forces and torques," *Advances in Space Research*, vol. 51, no. 1, pp. 10–20, Jan. 2013.

[29] W. R. Smythe, *Static and Dynamic Electricity*, McGraw–Hill, 3rd edition, 1968.

[30] Josip Sliško and Raúl A. Brito-Orta, "On approximate formulas for the electrostatic force between two conducting spheres," *American Journal of Physics*, vol. 66, no. 4, pp. 352–355, 1998.

[31] Trevor Bennett and Hanspeter Schaub, "Touchless electrostatic three-dimensional detumbling of large geo debris," in *AAS/AIAA Spaceflight Mechanics Meeting*, Santa Fe, New Mexico, Jan. 26–30 2014, Paper AAS 14-378.

[32] W. H. Clohessy and R. S. Wiltshire, "Terminal guidance system for satellite rendezvous," *Journal of the Aerospace Sciences*, vol. 27, no. 9, pp. 653–658, Sept. 1960.

[33] T. Bennett and H. Schaub, "Continuous-time modeling and control using linearized relative orbit elements," in *AAS/AIAA Astrodynamics Specialists Conference*, Vail, CO, August 9-13 2015.

[34] Erik Hogan and Hanspeter Schaub, "Space weather influence on relative motion control using the touchless electrostatic tractor," in *AAS/AIAA Spaceflight Mechanics Meeting*, Santa Fe, New Mexico, Jan. 26–30 2014, Paper AAS 14-425.